Regulation of DNA Repair Fidelity by Molecular Checkpoints: "Gates" in DNA Polymerase β's Substrate Selection†

Ravi Radhakrishnan,‡,§ Karunesh Arora,‡,|| Yanli Wang,‡ William A. Beard,⊥ Samuel H. Wilson,⊥ and Tamar Schlick*,‡

Department of Chemistry and Courant Institute of Mathematical Sciences, New York University, New York, New York 10012, and Laboratory of Structural Biology, National Institute of Environmental Health Sciences, National Institutes of Health, Research Triangle Park, North Carolina 27709

Received July 5, 2006; Revised Manuscript Received October 10, 2006

ABSTRACT: With an increasing number of structural, kinetic, and modeling studies of diverse DNA polymerases in various contexts, a complex dynamical view of how atomic motions might define molecular "gates" or checkpoints that contribute to polymerase specificity and efficiency is emerging. Such atomic-level information can offer insights into rate-limiting conformational and chemical steps to help piece together mechanistic views of polymerases in action. With recent advances, modeling and dynamics simulations, subject to the well-appreciated limitations, can access transition states and transient intermediates along a reaction pathway, both conformational and chemical, and such information can help bridge the gap between experimentally determined equilibrium structures and mechanistic enzymology data. Focusing on DNA polymerase β (pol β), we present an emerging view of the geometric, energetic, and dynamic selection criteria governing insertion rate and fidelity mechanisms of DNA polymerases, as gleaned from various computational studies and based on the large body of existing kinetic and structural data. The landscape of nucleotide insertion for pol β includes conformational changes, prechemistry, and chemistry "avenues", each with a unique deterministic or stochastic pathway that includes checkpoints for selective control of nucleotide insertion efficiency. For both correct and incorrect incoming nucleotides, pol β's conformational rearrangements before chemistry include a cascade of slow and subtle side chain rearrangements, followed by active site adjustments to overcome higher chemical barriers, which include critical ion−polymerase geometries; this latter notion of a prechemistry avenue fits well with recent structural and NMR data. The chemical step involves an associative mechanism with several possibilities for the initial proton transfer and for the interaction among the active site residues and bridging water molecules. The conformational and chemical events and associated barriers define checkpoints that control enzymatic efficiency and fidelity. Understanding the nature of such active site rearrangements can facilitate interpretation of existing data and stimulate new experiments that aim to probe enzyme features that contribute to fidelity discrimination across various polymerases via such geometric, dynamic, and energetic selection criteria.

DNA polymerases are essential for maintaining genomic order during DNA replication and repair (*1*) and thus for the long-term survival of a species. When DNA damage arising from a variety of exogenous and endogenous sources (e.g., environmental chemicals, radiation, and thermal aberrations) is not accurately repaired, it can lead to genetic alterations and eventually to human diseases like colon or skin cancer and premature aging (*2*, *3*). Thus, understanding polymerase fidelity mechanisms in DNA synthesis represents a fundamental biological and biomedical challenge. The fidelity of DNA polymerases broadly refers to their ability to incorporate correct rather than incorrect nucleotides complementary to the template DNA; such fidelities span a wide range, from one (in the case of Taq DNA polymerase) to nearly 1 million (for African swine fever virus pol X) errors per 1 million nucleotides incorporated (*4*).

Closed and open active site conformations of polymerases have been observed by X-ray crystallography and are often related by a large subdomain motion of the thumb in left-handed polymerases or, correspondingly, fingers in right-handed enzymes. An induced-fit mechanism (*5*−*10*) between the DNA-bound polymerase and the correct incoming nucleotide substrate leads to a "closed" tightly bound enzyme−substrate complex in which catalytic groups are

† This work was supported by NSF Grant MCB-0316771, NIH Grants R01 GM55164 and R01 ES012692, and the donors of the American Chemical Society Petroleum Research Fund (to T.S.), as well as the Intramural Research Program of the National Institute of Health, National Institute of Environmental Health Sciences (to S.H.W.). Research described in this article was also supported in part by Philip Morris USA Inc. and by Philip Morris International through an award to T.S.

* To whom correspondence should be addressed. Telephone: (212) 998-3116. Fax: (212) 995-4152. E-mail: schlick@nyu.edu.

‡ New York University.

§ Current address: Department of Bioengineering, University of Pennsylvania, Philadelphia, PA 19104.

|| Current address: Department of Molecular Biology, TPC-6, The Scripps Research Institute, 10550 N. Torrey Pines Rd., La Jolla, CA 92037.

⊥ National Institutes of Health.

10.1021/bi061353z CCC: $33.50
Published on Web 12/01/2006

Table 1: Rate-Limiting Step in Correct and Incorrect Insertions by DNA Polymerases (*10*, *20*, *21*)

		rate-limiting step	
polymerase	family	correct incorporation (pulse-chase, quench)	incorrect incorporation (thio effect)
Klenow fragment (KF)	A	conformational change	phosphoryl transfer
T7 DNA polymerase	A	conformational change	phosphoryl transfer
T4 DNA polymerase	B	phosphoryl transfer	conformational change
HIV-RT	RT	conformational change	conformational change
pol β	X	not determined	phosphoryl transfer
Dpo4	Y	conformational change	phosphoryl transfer

aligned as required for proper synthesis ("fidelity"); on the other hand, an incorrect incoming nucleotide leads to a DNA−polymerase complex with misaligned components so that synthesis is hampered. After synthesis, involving chemical incorporation of a nucleotide into DNA by means of phosphodiester bond formation (*11*), the enzyme complex releases PP_i and returns to its "open" state, to allow translocation for the next cycle of polymerization.

Common to several DNA and RNA polymerases (*11*−*13*), the covalent step of nucleotide incorporation (phosphodiester bond formation) occurs via the "two-metal-ion" catalyzed phosphoryl transfer mechanism. Experimental and theoretical evidence suggests that the resulting attack of the nucleophilic oxygen anion (O3′) on the target phosphorus (P_α) proceeds through a conformation resembling a trigonal−bipyramidal transition state formed by a penta-covalent phosphorus intermediate (*13*−*15*). Recently, direct structural evidence based on X-ray crystallography of a partially associative transition state in β-phosphoglucomutase was reported, in which the critical distance between the nucleophilic oxygen and the target phosphorus was 2.0 Å (*14*).

Throughout this article, we divide the process of nucleotide insertion into three steps, each of which can involve substeps: the protein and DNA conformational changes, prechemistry changes, and the chemical step. The conformational changes are defined as the trajectory that brings the system from an open to closed state as described by X-ray crystallography (see ref *7* for pol β). Prechemistry follows to bring the system into its reaction-competent state, and then chemistry involves incorporation of the incoming nucleotide into the primer strand. We divide what is typically called "chemistry" into both prechemistry and chemistry steps because these regions may be characteristically different, in the sense that the former involves stochastic barrier hopping rather than a dominant pathway, which may occur for the chemical reaction itself; this separation also allows us to interpret differing mechanisms among different polymerases.

Recently, Joyce and Benkovic (*10*) reviewed the structural and kinetic data for correct and incorrect dNTP (2′-deoxyribonucleotide 5′-triphosphate) incorporations by a variety of DNA polymerases. Their summary shows that, despite common threads, no unified description describes the overall reaction profile of these enzymes (Table 1, with additions). For example, the noncovalent, conformational change step (involving a large subdomain motion) prior to nucleotide incorporation is common among a wide range of polymerase systems, but whether this step or the chemical step is rate-limiting during correct or incorrect nucleotide incorporation differs case by case; see ref *10* and references therein. Four general possible scenarios for the rate-limiting step for both correct and incorrect dNTPs have been delineated (*16*). Namely, the rate-limiting step might be the (i) conformational change for correct but chemical step for incorrect units, (ii) chemical step for correct but conformational change for incorrect units, (iii) conformational change for both, or (iv) chemical step for both. These details are important because differences in free energy barriers corresponding to the rate-limiting steps of correct and incorrect nucleotide incorporation can be used to calculate fidelity. Still, such energetics alone are insufficient to understand the complexity of polymerase mechanisms. The structure−flexibility−function relationships that define the major barriers, which in turn represent kinetic checkpoints or "gates" to the respective molecular mechanisms and interactions, are essential for unraveling the incorporation events at atomic and molecular levels.

For two well-studied DNA polymerases (Klenow fragment and T7 pol), available kinetic data have been interpreted as showing that the noncovalent step preceding phosphoryl transfer is rate-limiting for correct dNTP incorporation, while phosphoryl transfer is rate-limiting for an incorrectly paired incoming dNTP incorporation (*10*). As seen in Table 1, a consistent pattern is lacking. Interpretations are further obfuscated by the fact that the thio-elemental effect (the decrease in rate when an α-thio-dNTP is substituted for the normal all-oxygen nucleotide) may not be reliable for identifying a rate-limiting phosphoryl transfer step (*10*, *17*). For polymerases like pol β, for which the evidence for a slow step preceding phosphoryl transfer is based largely on elemental effect arguments and on the analogy to other systems, the assignment of this step as rate limiting in the reaction pathway is weak. For polymerases like the Klenow fragment, T7 pol, HIV-RT, and two Y-family polymerases yeast Pol η and archaeal Dpo4, however, more persuasive evidence favors a slow noncovalent step preceding chemistry when a correctly paired dNTP is added (Table 1). In these polymerases, the lower yield from pulse-quench versus pulse-chase protocols indicates the presence of a dNTP-bound species that can form product instead of dissociating and equilibrating with the pool of free dNTP (*10*).

Fluorescence-based techniques have been employed to infer the time scales of conformational change in DNA polymerases. In particular, for pol β, the time scale for fluorescence was compared with the overall rate of nucleotide incorporation to infer the rate-limiting step. However, different studies by the same group gave contrasting results regarding the rate-limiting step (*18*, *19*). The experimental uncertainty is further compounded by the fact that the origins of the fluorescence changes are often speculative and the absence of a fluorescence change may simply reflect the fact that the probe is not positioned to monitor relevant events.

Clearly, the complexity and diversity of DNA polymerase mechanisms require, in addition to structural and kinetic studies of DNA polymerases (*10*, *12*, *22*−*25*), a detailed atomic-level dynamic and energetic view of how sequential structures and motions define gates or checkpoints in the mechanistic landscape. Such details are necessary for a full interpretation of polymerase specificity and efficiency. With recent advances in simulation methodology and computer power, valuable information is within reach in molecular modeling and dynamics simulations well grounded in available data, e.g., (*26*−*28*). In addition, dynamical experimental information from NMR that probes the conformational dynamics of the polymerase and its substrates, as carried out recently (*29*, *30*), is crucial in defining this dynamical landscape. Insights into rate-limiting conformational and chemical steps can emerge from new information concerning transition states and transient intermediates along a reaction pathway. By systematically comparing behavior for correct and incorrect incorporation and extension before and after the chemical reaction, we can piece together geometric, thermodynamic, and dynamic factors that contribute to polymerase function. Indeed, recent simulation studies supported by various site-directed mutagenesis experiments have suggested that, rather than simple subdomain rearrangements, subtle active site conformational changes direct pol β's catalytic pathway.

Here we describe this emerging pathway for pol β while mentioning related regulation issues relevant to other polymerases. Namely, we collect geometric, energetic, and dynamic features that have emerged as key players governing fidelity mechanisms of DNA polymerases as gleaned from computational studies (*26*−*28*, *31*−*36*). Most interesting in this landscape is that part of the pathway we call the prechemistry "avenue" which involves high barriers that evolve as the enzyme moves to the reaction competent state. Though details of these changes vary among polymerases, an understanding of the associated geometric and energetic factors for pol β may serve as a reference framework for interpreting polymerase cycles more broadly.

DNA POLYMERASE β

Evidence of Induced Fit from Structural and Kinetic Studies. X-ray crystallography has provided exquisite views of pol β frozen in action: closed (active) and open (inactive) forms of the enzyme related by a large subdomain motion of the thumb (*7*). Together with kinetic studies of pol β, the implied "induced-fit" mechanism, in which the correct incoming base triggers the requisite conformational change while an incorrect incoming nucleotide hampers the process, has gained support from a variety of dynamics simulations. Enzyme systems where the active site is occupied by the correct substrate trigger a thumb subdomain closing motion with the alignment of active site protein residues that favors the subsequent chemical step (*27*, *33*); in contrast, the absence of the substrate (*33*) leads to a thumb opening motion and is accompanied by local rearrangements near the active site that disfavor the chemical step. Simulations with mismatches (*32*) reveal a hierarchy of closing trends that mirror experimental data (*37*, *38*).

Studies on another family X member, pol X, which lacks the "fingers" subdomain, also support the induced-fit mechanism (*39*). Here, two available DNA-free NMR structures

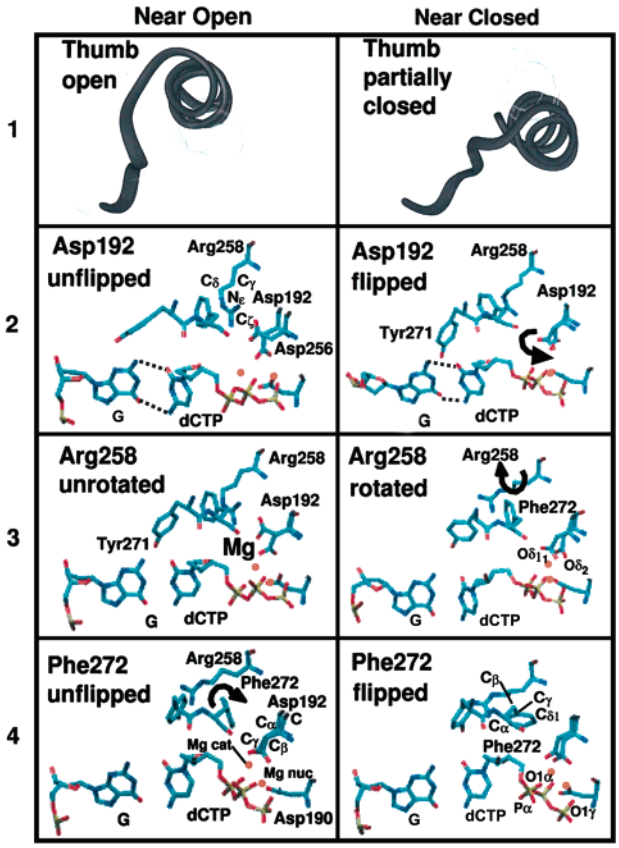

FIGURE 1: Molecular snapshots near open (left) and closed (right) states for four transition state regions in pol β's open to closed conformational change revealed by transition path sampling: (1) partial thumb closing, (2) Asp192 flip, (3) Arg258 partial rotation, and (4) Phe272 flip.

(*18*, *40*) served as anchors, as well as two modeled DNA−pol X complexes provided by M. D. Tsai, one containing gapped DNA and the other gapped DNA with an incoming base; only with the DNA and incoming nucleotide in the active site does pol X exhibit a conformational change toward a closed state. Interestingly, the work also suggests that the two NMR structures interconvert to one another under physiological salt conditions (*39*). Furthermore, simulations on pol λ (*41*), another family X member with fidelity lower than that of pol β, reveal that a loop in the thumb subdomain and DNA as well as active site residues also undergo conformational changes to prepare the active site for the chemical reaction only when the correct incoming nucleotide and ions bind to the primer−template terminus. This suggests that the induced-fit mechanism might also contribute to the maintenance of pol λ's fidelity.

Transient Intermediates of the Conformational Pathways. The global subdomain motions of pol β are accompanied by a complex cascade of sequential side chain motions and active site rearrangements that are highly sensitive to the active site content and environment (e.g., ions). In particular, transition path sampling simulations reveal a complex geometric−energetic landscape (Figures 1 and 2) associated with pol β's thumb closing (*27*) and help identify "gatekeeping" residues that may direct polymerase action. Overall, the five identified transition states (TS) extend available experimental and modeling data by revealing highly cooperative dynamics and critical roles of many key residues (Arg258, Phe272, Asp192, and Tyr271).

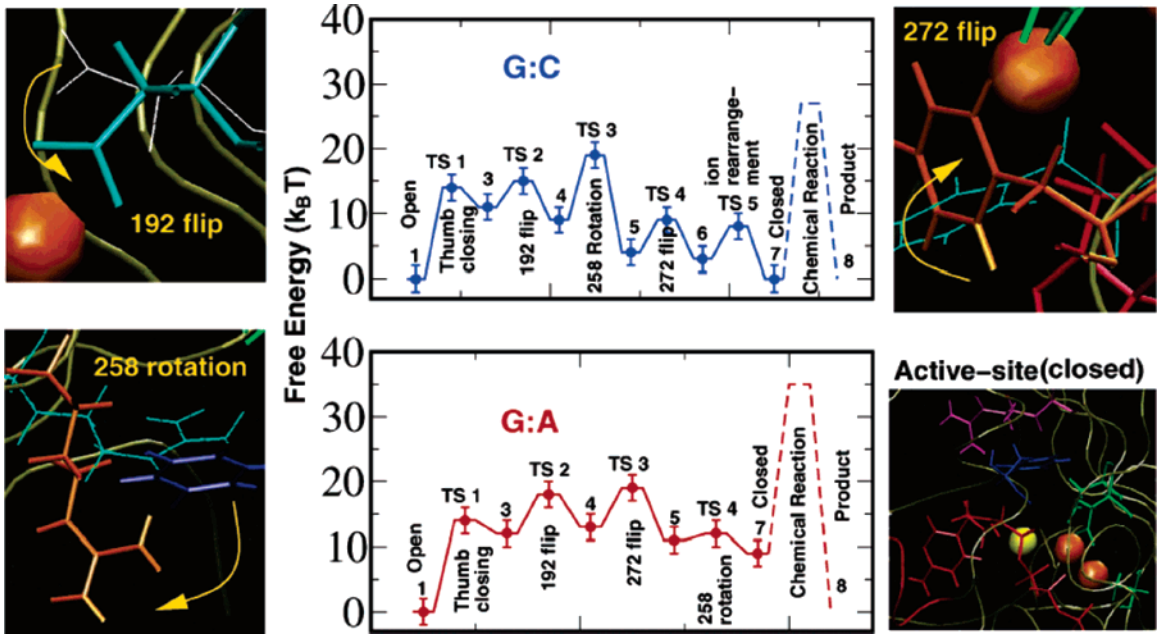

FIGURE 2: Reaction profiles for the closing conformational change before phosphoryl transfer in G·C and G·A systems of pol β.

The collective cascade of the sequential geometric rearrangements following partial thumb closing, including Asp192 flip, Arg258 rotation, and Phe272 rotation (Figures 1 and 2), brings the DNA and correct dNTP-bound pol β system to a state nearly competent for the chemical reaction and suggests how subtle residue motions and conformational steps affect reaction efficiency and fidelity; this system of checks and balances directs the system to the chemical reaction and likely facilitates enzyme discrimination of the correct from the incorrect incoming nucleotide. Together with the chemical reaction, these conformational features are central to the dual nature of polymerases, requiring specificity (for correct nucleotide selection) and versatility (to accommodate different templates at every step). The specific energy barriers involved (Figure 2) are discussed in Mismatch Incorporation in Pol β and Divalent Magnesium Ion Landscape.

Besides the orchestrated conformational pathway before chemistry that is critical for DNA replication fidelity, studies have also shown that kinetic checkpoints exist after the chemical reaction. Pioneering work on the large fragment of *Bacillus stearothermophilus* DNA polymerase I (BF) by Beese and co-workers has provided a tantalizing series of snapshots of nucleotide incorporation in a family-A DNA polymerase (*42*). Namely, mismatch recognition interactions considerably impede the DNA extension of a mispair at a postinsertion site (i.e., primer terminus). A similar structural and kinetic interpretation for pol β has been described previously (*38*, *43*).

Computational studies after the chemical reaction for pol β (*26*, *34*−*36*) suggest a sequence of molecular events during the enzyme's opening: flipping of the Phe272 ring, movement of the thumb, and rotation of Arg258 toward Asp192. By comparing the computationally calculated rates to experimental incorporation rates (k_{pol}) of 1−10 s^{-1} (*37*, *44*), one can argue that the local structural rearrangement involving Arg258 rotation is slow relative to subdomain motions, as previously assumed (*22*).

That thumb opening after chemistry in the matched G·C complex occurs much faster compared with the closing before chemistry (*26*, *33*) might explain in part the difficulty in performing pulse-chase experiments to determine whether the substrate ternary complex is in rapid equilibrium with the polymerase−DNA binary complex. That is, if events following chemistry are fast (regardless of whether a slow conformational change before chemistry exists), then the E*−DNA−dNTP complex cannot accumulate and a difference in quenching agents (HCl or cold dNTP) will not reveal the slow conformational transition.

Mismatch Incorporation by Pol β. The exploration of the role of induced fit in substrate selection also requires the study of nucleotide misincorporation events. Experimental progress on this front has been limited due to the instability of these mismatched complexes in the active state and the complexity surrounding interpretation of the (thio) elemental substitution on the rates of misincorporation (*10*, *17*). At the same time, modeling mismatches is challenging because assumptions made regarding initial geometry, ion coordination, and other interacting residues influence resulting pathways. Ideally, modeling mismatches requires consideration of four possible conformations (*anti*:*anti*, *syn*:*anti*, *syn*:*syn*, and *anti*:*syn*) for each mismatch, with preferences gleaned from free DNA and related protein−DNA complexes. However, because atomic-level simulations and free energy calculations for enzymes like polymerases with highly charged DNA and metal ions are very demanding in computing resources, the *anti*:*anti* conformation is assumed most likely and simulated in practice. Still, dynamics simulations of mismatches can reveal interconversion of orientations when dictated by the active site and environment (*36*) and help reveal geometric, structural, and energetic aspects distinct from those of matched systems.

Several computational studies have examined the structural changes and polymerase−substrate interactions with matched and mismatched base pairs in the polymerase active site (*26*, *28*, *31*, *45*, *49*). Specifically, dynamics simulations of pol β

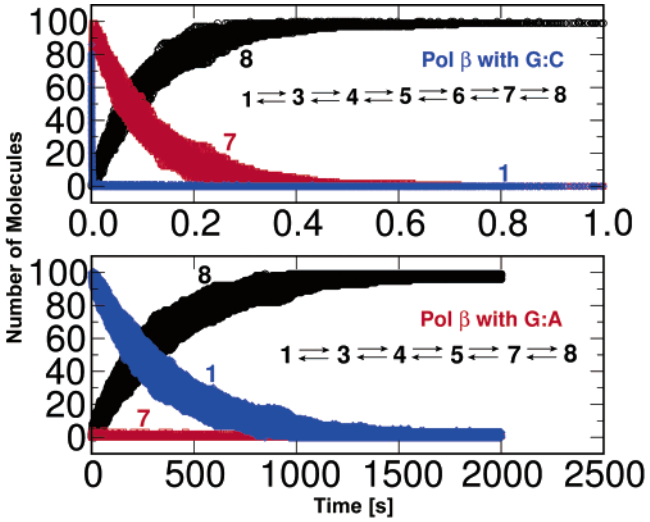

FIGURE 3: Reaction profiles for conformational changes before phosphoryl transfer in G·C and G·A systems of pol β. Details can be found in ref *28*. Numerals 1, 3−5, 7, and 8 correspond to the metastable states defined in Figure 2.

complexed with mispairs (template:incoming, G·G, G·T, and T·T) at the template−primer terminus before the chemical reaction indicate that mismatch systems tend toward the open conformation observed in the binary pol β structure with gapped DNA rather than the closed form preferred by the correct-base-pair complex (G·C); the extent of thumb closing in these complexes with respect to the crystal closed conformation can be ranked as follows: G·G < T·T < G·T < G·C. Furthermore, the degree of distortions in the active site geometry of the mismatches (in increasing order, G·T < G·G ~ T·T) matches the experimentally determined efficiencies of misincorporation (*38*) for different mismatches. This finding suggests that the structural distortion in the active site introduced by the mispairs is correlated with pol β fidelity. Because most DNA polymerases insert incorrect nucleotides with similar efficiencies (*4*), such discrimination might apply to other polymerases.

Simulations of pol β subsequent to incorrect nucleotide incorporation (*26*) help interpret kinetic data for DNA mispair extension. Because active site geometries of different mispairs form a hierarchy which parallels the experimentally deduced inefficiency of pol β to extend these mispairs, such local distortions of mismatched base pairs could impede DNA extension and lead to proofreading by an extrinsic exonuclease.

In addition to the dynamics simulations, transition path sampling has uncovered the differing conformational pathways of pol β's thumb closing for correct dCTP versus incorrect dATP incoming nucleotide opposite a template G (*27*, *28*) (Figure 2). The overall free energy barriers for the matched and mismatched complexes are comparable to one another (both $19 \pm 3 \times k_BT$), but the closed G·A state is less stable than its open state by $9k_BT$, unlike the G·C complex, in which the closed state is as stable as the open state.

On the basis of free energy profiles, the overall insertion rates for the G·C and G·A complexes can be evaluated by a network model of elementary chemical reactions (*28*). Results (Figure 3) indicate that the mismatch G·A complex stays in the open state longer than the closed conformation, compared to the fast active site assembly process resulting from a stable closed state in the matched G·C complex. Thus, the different sequences of transition states in the correct versus incorrect base pair complexes dictate different conformational pathways toward an ideal "two-metal-ion catalysis" geometry.

In this connection, experimental work on assessing the role of Watson−Crick hydrogen bonding is noteworthy. This work demonstrates that the role of these hydrogen bonds for substrate discrimination during DNA synthesis appears to be DNA polymerase-dependent. Specifically, Kool and coworkers have employed fluorinated nucleoside isosteres in separating the contributions of hydrogen bonding at the Watson−Crick edge and minor groove of the nascent base pair from the steric and geometric constraints imposed by the nascent base pair binding pocket (*46*). Moran and Kool (*47*) first described the efficient and specific replication of difluorortoluene (DFT) by an exonuclease-deficient mutant of the Klenow fragment of *Escherichia coli* DNA polymerase I; that work suggested that Watson−Crick and polymerase−template nucleotide hydrogen bonding was dispensable during substrate discrimination for this A-family DNA polymerase. In contrast, Morales and Kool (*48*) later found that pol β did not insert the sterically complementary dATP opposite DFT. Using [*methyl*-^{13}C]methionine-labeled pol β to probe the conformational response of the enzyme to homologous substrates containing either thymine or DFT at the templating base position, Kirby et al. demonstrated that replacing a templating thymine base with a DFT residue repressed the large conformational transition associated with formation of a closed active complex (*30*). It remains to be determined whether this is due to a requirement for Watson−Crick hydrogen bonding within the nascent base pair or whether critical hydrogen bonding with the minor groove edge of the template base is essential for stabilizing the closed polymerase conformation.

Our MD simulations on different mismatches indicate that the bulkiness (shape) of the mispair and possible hydrogen bonds between the two bases as well as between the triphosphate and pol β are main factors determining the stability of the closed states. The active site residues binding the triphosphate (Arg183, Ser180, and Gly189) might be particularly crucial for the conformational change (see Prechemistry Avenue for further discussions). In particular, we note that the origin of the differences in stability between the correct G·C and incorrect G·A systems stems from two key interactions (*28*): (1) electrostatic stabilization at the active site provided by Arg283, and (2) the favorable ligand complexation involving the conserved aspartates and the catalytic Mg^{2+}. In the correct system, the active site conformation capitalizes on an energetic advantage based on these interactions. For the incorrect G·A system, the bulky purine·purine mispair disrupts the assembly of an ideal two-metal-ion active site and leads to a more distorted geometry for which the favorable electrostatic interaction is weakened compared to that of the correct system. These energetic traits are reflected in the reduced stability of the active state (in the conformational closing free energy profile) for the incorrect G·A system compared to the correct G·C system.

Mutant Studies of Pol β. Experimental and computational studies have identified a series of key residues at or near the active site of pol β with suggested roles (Table 2).

Table 2: Key Residues of Pol β and Their Roles in the DNA Replication Cycle

	role					
residue	conformational closing before chemistry	prechemistry	conformational opening after chemistry	effect[a] on fidelity	ref (exptl)	ref (computational)
Ser180	interacts with the γ-phosphate of the incoming dNTP	interacts with the γ-phosphate of the incoming dNTP	releases the H-bond with the pyrophosphate	S180A, NE	*54*	
Arg183	interacts with the β-phosphate of the incoming dNTP	interacts with the β-phosphate of the incoming dNTP	releases the H-bonds with the pyrophosphate	R183A, NE	*54*, *55*	
Gly189	interacts with the γ-phosphate of the incoming dNTP	interacts with the γ-phosphate of the incoming dNTP	releases the H-bond with the pyrophosphate	G189A, ND	*56*	
Asp190	coordinates with the two metal ions	subtly rearranges to coordinate the two metal ions	releases interactions with the two metal ions	D190S, ND; D190E, ND	*56*	*28*
Asp192	flips away from Arg258 and binds the two metal ions	subtly rearranges to coordinate the two metal ions	side chain flips away from the active site	D192S, ND; D192E, ND	*56*	*27*, *28*, *34*
Asp256	interacts with the catalytic Mg^{2+} and O3′ of the DNA primer	rearranges to coordinates catalytic Mg^{2+}, the primer terminus, and α-phosphate	releases binding with the catalytic Mg^{2+} and the primer terminus	D256A, ND	*57*	*28*
Arg258	rate-limiting motion, gatekeeping mechanism, motion coordinated with thumb closing	interacts with Glu295/Tyr296, away from the active site	rate-limiting motion coordinated with thumb opening, interacts with Asp192	R258A, NE	*57*; Wilson et al., unpublished results	*26*, *27*, *35*
Tyr265	present in the hydrophobic hinge region of the C-terminal domain; involved in thumb closing	involved in precise geometric ordering of the active site	involved in thumb opening	Y265C, 23-fold↓; Y265H, 117-fold↓; Y265F, NE; Y265W, NE	*44*, *58*, *59*, *60*	
Tyr271	interacts with the primer terminus nucleotide base and the nascent base pair	interacts with the nascent base pair as well as the primer terminus nucleotide base	interacts with the nascent base pair	Y271A, NE; Y271F, 3.4-fold↓; Y271F, NE; Y271H, NE; Y271S, 3.5-fold↓;	*54*, *61*	*27*, *35*
Phe272	insulates the salt bridge between Arg258 and Asp192; motion coordinated with thumb closing	blocks the interaction between Arg258 and Asp192	side chain flips away from the active site	F272L, 2.2-fold↓	*62*	*26*, *28*, *35*
Asp276	interacts with the incoming dNTP base and Arg40 of the lyase domain in the closed state	interacts with the incoming dNTP base	moves away from the incoming dNTP base	D276V, ND; D276E, 8.8-fold↓	*37*, *63*	*35*
Asn 279	interacts with the template base and compensates for the loss of interactions involving residue 271 in mispair and mutant systems	interacts with the template base and compensates for the loss of interactions involving residue 271 in mispair and mutant systems	interacts with the template base and compensates for the loss of interactions involving residue 271 in mispair and mutant systems	N279A, 8.7-fold↑; N279A, 2.1-fold↓; N279L, 2.0-fold↑; N279Q, 2.7-fold↓	*54*, *61*	
Arg283	interacts with the template base	interacts with the template base	moves away from the template base	R283A, 164-fold↓; R283A, 37-fold↓; R283K, 15-fold↓; R283L, 89-fold↓	*61*, *64*, *65*	*27*, *35*
Glu295	forms a H-bond with Arg258	forms a H-bond with Arg258	releases the H-bond with Arg258	E295A, 4.6-fold↓	*54*	
Tyr296	forms a H-bond with Arg258	forms a H-bond with Arg258	releases the H-bond with Arg258			

[a] Effects are averaged over the number of observations from different groups and the different mispairs that were examined: ND, not determined; NE, no effect (a <2-fold difference); ↑, fidelity increase; ↓, fidelity decrease.

Numerous mutagenesis experiments have described the effects of localized mutations (Y271F, Y271H, D276V, R283A, R283K, R283L, R258A, and R258K) on the enzyme's efficiency and fidelity (see Table 3) (*50*). Dynamics simulations for various pol β mutants (*35*) also provide critical insights into the functions of these residues in atomic detail and help in the interpretation of the kinetic data.

In the computational studies of pol β−DNA complexes that captured the complete thumb transitions (*26*−*28*, *31*−*36*), Arg258 emerged as the slowest substep in the conformational pathway. Recent experimental studies of pol β and Klentaq1 DNA polymerase also suggest that subdomain motions in polymerases are relatively fast compared to side chain motions (*51*, *52*). Further evidence for the role of Arg258 as a kinetically important residue during conformational closing comes from recently determined crystal structures of pol λ, an X family member, bound to a two-nucleotide gapped DNA (*53*). Intriguingly, the crystal structure indicates that pol λ is in a closed conformation without a bound incoming unit (dNTP); the presence of Ile492 in pol λ in the position corresponding to Arg258 in pol β was used to explain the limited interactions of pol λ with primer−template DNA and its low barrier to closing (*53*). In dynamics studies on pol λ, Ile492 emerges as a residue that helps move the system from binary to ternary states by determining the position of neighbor residue Phe506 (Phe272 in pol β) (*41*).

Arg258 in pol β is located in the microenvironment of the incoming nucleotide (see Figure 4). Crystal data (*7*) have shown that during nucleotide binding prior to the chemical reaction, Arg258 undergoes a rotation away from Asp192, which is thus freed to chelate two functional Mg^{2+} ions for the catalysis of the nucleotidyl transfer reaction. Kinetic data (*57*) also indicate that the R258A mutant decreases the efficiency of dNTP binding but not the chemical step. A series of computational studies by molecular dynamics and transition path sampling before chemistry on the mutant enzyme R258A (Appendix A of the Supporting Information)

Table 3: Kinetic Data for Wild-Type Pol β and Pol β Mutants on Fidelity and Catalytic Activity

	rate constant k_{pol}[a,b] (s^{-1})	fidelity[a,c]	catalytic efficiency[a] k_{pol}/K_d[d] (M^{-1} s^{-1})	dNTP binding affinity K_d[d] (μM)	ref
WT	9.4−24	1600−51000	125000−1100000	8.6−108	*64*
R283A	0.048−0.83 (decreased)	150−6800 (decreased)	340−4900 (decreased)	61−170 (increased)	
WT	3.4−17	3900−51000	180000−510000	6.7−66	*54*
Y271A	0.58−4.1 (decreased)	3400−21000 (similar)	290000−415000 (similar)	1.4−8.0 (decreased)	
WT (G·dCTP)	10.0	N/A[e]	1790000	5.6	*37*
D276V (G·dCTP)	6.3 (decreased)	N/A[e]	10500000 (increased)	0.6 (decreased)	

	k_{pol}[b] (s^{-1}) (T·dATP)	fidelity[c] (T·dGTP)	K_d[d] (μM)	K_m[f] (μM)	k_{cat}[g] (s^{-1})	k_{cat}/K_m (M^{-1} s^{-1})	ref
WT	7.6	4400	4.6	1.1	0.9	820000	
R258A	18.0 (increased)	9300 (increased)	25 (increased)	7.9 (incresead)	1.8 (incresead)	230000 (decresead)	Wilson et al., unpublished results
R258K	N/A[e]	N/A[e]	N/A[e]	9.8 (increased)	1.7 (increased)	173000 (decreased)	Wilson et al., unpublished results

[a] Ranges reflect the different base pairs that were experimentally investigated; single values refer to a specific base pair for both the mutant and wild type. [b] k_{pol} is the rate of nucleotide incorporation for first-enzyme turnover. [c] K_d is the apparent equilibrium dissociation constant of dNTP. [d] Fidelity = $(k_{cat}/K_m)_c/(k_{cat}/K_m)_i$, where c and i denote incorporation of the correct and incorrect nucleotide, respectively. [e] Not available. [f] $K_m = K_d$ if k_{pol} is the rate-limiting step. [g] k_{cat} measures the slowest step, or steps, in the reaction cycle during a steady state assay.

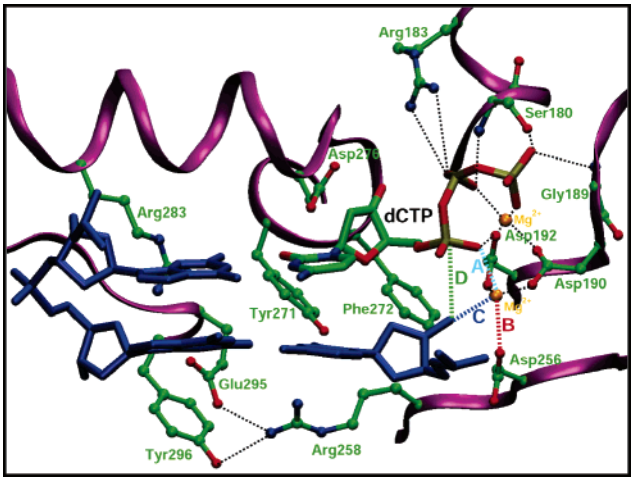

FIGURE 4: Active site of pol β in the closed complex (*7*) as rendered by VMD (*66*). Black dashed lines represent the hydrogen bonds and the coordination of the catalytic and nucleotide-binding Mg^{2+}. Key P_α−O3′, Mg^{2+}(cat)−O3′, Mg^{2+}(cat)−O1α, and Mg^{2+}(cat)−OD2 Asp256 distances are labeled A−D, respectively.

suggest that the closing of pol β is accelerated when Arg258 is mutated to alanine, fitting well with kinetic measurements regarding the increased rate of nucleotide insertion in R258A relative to that of the wild-type enzyme (Wilson et al., unpublished data). Namely, the simulations for R258A suggest that the thumb moves toward a closed state at a rate much faster than that of the wild-type pol β simulation (*33*). The free energy landscape corresponding to TS3 for the wild-type enzyme depicts a barrier of $13k_BT$ for the rotation of Arg258 (Figure 2). Elimination of this barrier in R258A suggests an overall barrier lowered by $\sim 3k_BT$ (difference between TS3 and TS2). This translates into 3−4-fold enhancement in the overall rate of incorporation for R258A and explains the increased rate of nucleotide insertion in R258A relative to that in the wild-type enzyme.

Modeling work also helps clarify the structural effects of several key residues on pol β's opening after the nucleotidyl transfer reaction. Studies of five single-residue mutants [R283A, Y271A, D276V, R258K, and R258A (*35*)], selected due to hypothesized roles in maintaining fidelity, nucleotide binding affinity, and/or catalytic efficiency, indicate that all mutant systems except R258A (which approaches the closed rather than open state) delay the thumb's opening. The stable closed form of R258A resulting from removal of the hydrogen bond between Arg258 and Asp192 echoes facilitated thumb closing in the simulation of this mutant before chemistry, explaining the increased rate of nucleotide incorporation in this mutant with respect to that of the wild-type enzyme. Furthermore, the altered interactions between mutated residues and the newly incorporated incoming nucleotides in simulated mutant complexes help in the interpretation of the kinetic data with regard to nucleotide binding affinity in R283A (decreased), Y271A (slightly increased), D276V (increased), and R258A (decreased) relative to that of the wild type. Specifically, in R283A and R258A, decreased interactions between the nascent base pair and residues 283 and 258 are consistent with the nucleotide binding affinity being weakened compared to that of the wild-type enzyme. In D276V, increased interactions between the incoming nucleotide and Val276 might account for the stronger nucleotide binding affinity. In Y271A, however, the diminished interaction between residue 271 and the incoming nucleotide is not consistent with the increased nucleotide binding affinity. It is possible that interactions between certain active site residues (e.g., Phe272, Asn279, and Arg283) adjacent to residue 271 and the incoming nucleotide may compensate for the loss of the Tyr271−nucleotide interaction and thereby increase the nucleotide binding affinity in Y271A.

These studies on mutants again reinforce the dual nature of DNA polymerases, versatility and specificity of the active site, in accommodating various nucleotides while preserving fidelity. These combined works provide insights into dynamic and structural aspects of the active site environment at the atomic level and emphasize the highly organized but pliant active site essential to the chemical reaction of nucleotide incorporation.

Divalent Magnesium Ion Landscape. That polymerase function depends critically on the ionic microenvironment is well appreciated experimentally (*13*). The polymerase efficiency and fidelity are altered in the presence of noncognate ions such as Mn^{2+} when compared to a Mg^{2+} microenvironment (*67*). Although the degree of sequence similarity across families of DNA polymerases is low, the two-metal-ion (Mg^{2+}) coordination with conserved acidic residues (e.g., two highly conserved aspartates and an additional residue such as aspartate or glutamate) in the enzyme active site is a common feature (*68*). The conservation of the metal-binding site in highly divergent DNA polymerases underscores the importance of the metal ions in assisting nucleotide polymerization.

Experimental and simulation studies (*45*, *69*, *70*) have emphasized the functions of the metal ions in the nucleotidyl transfer reaction. Studies probing the effects of nucleotide-binding and catalytic Mg^{2+} ions on conformational changes in pol β before and after the chemical reaction (*34*) suggest that conformational closing before the chemical reaction is achieved and sustained only when both divalent metal ions are present in the active site while opening after the chemical reaction is triggered by release of the catalytic metal ion. Similar studies on DNA pol λ also reveal that a stable closed conformation in which active site residues are nearly aligned for chemistry can be achieved only in the presence of both metal ions (*41*).

However, it does not follow that only with both metal ions bound can large subdomain conformational transitions occur, but rather that both ions are necessary to stabilize the closed conformation. In a recent mechanistic enzymology study of pol β (*71*), Bakhtina et al. concluded that chemistry is the rate-limiting step for overall insertion and asserted that their results contradict the results from published computational studies (*26*, *27*, *34*) on mechanistic features of the nucleotide insertion pathway. However, the contradiction was deduced on the basis of an incorrect representation of our proposed pol β mechanism. Specifically, the Tsai group quoted directly from ref *34*, "the binding of the catalytic magnesium and the rearrangement of Arg258 may be coupled and represent a slow step in pol β closing before chemistry", where we discussed the conformational pathway and not the overall insertion reaction (i.e., conformational and chemistry avenues). Clearly, the word "slow" is not synonymous with "rate-limiting" for overall insertion, and any chemical barriers to insertion were not addressed in our work. However, from comparisons of the computed conformational barriers [overall barrier for the conformational change of $20.5 \pm 3 \times k_BT$ (*34*)] and the experimentally measured insertion rate in the literature [overall rate of the reaction, $\sim 25k_BT$, as obtained from experimental kinetic data; k_{pol}, the rate of nucleotide insertion of $1-10\ s^{-1}$ (*37*, *44*)], we in fact suggest that chemistry may be rate-limiting for the overall insertion pathway. This point was stated in ref *27* and reiterated in a later work, where it was concluded that "additional high-energy barriers must be overcome to reach the ideal geometry appropriate for the chemical reaction" (*31*−*33*) (see also subsection below on the chemistry step).

On the basis of stopped-flow fluorescence measurements, the Tsai group concluded that subdomain conformational closing in pol β occurs before metal ion binding, while the chemical step of nucleotide incorporation occurs after ion binding. On this basis, they asserted that their experimental observations on the sequence of events contradict reported computational studies. Again, as Bakhtina et al. (*71*) point out, the conformational change step and the chemical step can themselves involve multiple elementary steps or discrete states. As discussed here, the computational study in ref *34* dissected these elementary steps for the conformational change phase of pol β's cycle (see Figures 1 and 2). Importantly, these subtle, sequential transitions lead to tight binding of the catalytic magnesium ion at the active site. That is, the catalytic magnesium ion is bound properly only at the end of this cascade of events, which follows partial thumb closing.

Thus, modeling suggests that binding of both of the divalent metal ions is necessary to stabilize the closed conformational state of pol β, but this in no way implies that both metal ions must be bound to produce a fluorescence signal that arises because of movement of the thumb subdomain (*71*). While we cannot comment on the specific contributions of each transient state to the fluorescence intensity analyzed experimentally, the sequence of microscopic events involved in the conformational change, as gleaned from the computational studies, involves partial thumb closing followed by subtle side chain motions that result in binding of the catalytic magnesium ion along with stabilization of the closed conformation of pol β. Furthermore, results of experiments in an environment different than the native one [such as high-viscosity sucrose medium rather than water, deoxyribonucleoside triphosphate-α-S substrate instead of dNTP, and inert metal ion Rh(III) rather than divalent ions] cannot be directly compared with computational results. Thus, all modeling data, including the recent delineation of the chemical pathway (see Chemistry Step), point to chemistry as the likely rate-limiting step for pol β for both correct and incorrect systems but emphasize that subtle and sequential conformational events triggered by substrate binding steer the system to the active conformation required for chemistry.

Prechemistry Avenue. In the idealized two-metal-ion geometry, the catalytic and nucleotide-binding magnesium ions are octahedrally coordinated with O^- groups. The P_α of incoming dCTP is pentacoordinated such that the terminal oxyanion (O3′) of the primer DNA is in line with the bond between P_α and $O2_\alpha$. While such a conceptual picture of the two-metal-ion transition state has been accepted widely across several enzymes and ribozymes that catalyze a phosphoryl transfer reaction, the precise structural characterization of the transition state is limited to a few cases.

A computational study of the phosphoryl transfer reaction catalyzed by β-phosphoglucomutase by Webster (*72*) reveals that the crystal structure of Lahiri (*14*) is geometrically close to the transition state. However, the computational study notes that an additional activation barrier must be overcome for the crystal structure to reach the transition state (an activation process of ≥ 10 kcal/mol). The additional energetic penalty may come from the deprotonation of the attacking hydroxyl in forming the oxyanion. Nevertheless, the transition state identified by Webster possesses the key characteristics: the deprotonation of oxyanion, formation of a bond between the oxyanion and target phosphorus, and breaking of the bond to release the pyrophosphate. That the phos-

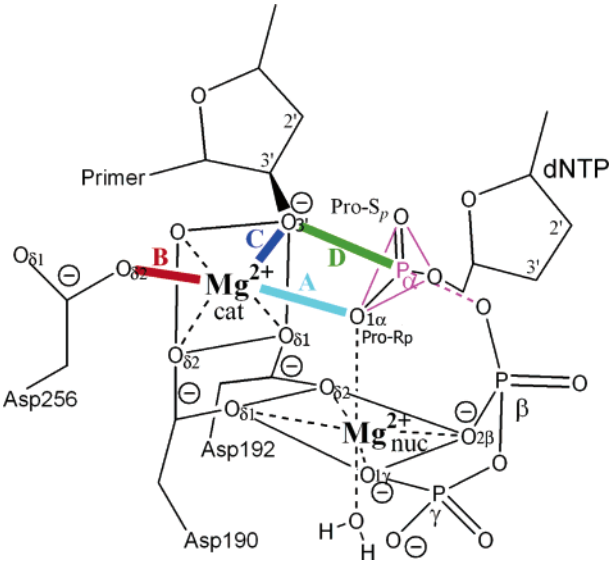

FIGURE 5: Active site of pol β depicting the pentacoordinated P_α of the incoming dNTP and the octahedrally coordinated catalytic and nucleotide-binding Mg^{2+}. Key distances are labeled A−D.

phoglucomutase scenario is functionally relevant to polymerase catalysis is reconciled by the striking similarity in the computed mechanisms of Webster for the former case and Warshel and co-workers for T7 DNA polymerase (*45*). The transition state identified by Warshel possesses the same key characteristics of the Webster results. Although Webster observed a simultaneous occurrence of these events, Warshel et al. found these to be temporally separate (i.e., three different transition states). However, the free energy barriers are strikingly close (10 kcal/mol reported by Webster vs 11 kcal/mol by Warshel).

The modeling results for the solvated pol β−DNA−dCTP ternary complex with a G·C base pair at the active site indicate that the geometry of a solvated, equilibrated structure deviates from the ideal geometry. The distances *A* [$O1_\alpha$−dCTP−Mg^{2+}(cat), 4.5 Å], *C* [O3′−Mg^{2+}(cat), >4.5 Å], and *D* (O3′−P_α, 2.0 Å) are all greater than their corresponding ideal values (2.0, 2.0, and <3.3 Å, respectively) (see Figure 5). Furthermore, critical distances *B* [Mg^{2+}(cat)−$O_{\delta2}$ (Asp256)], *C*, and *D* of the closed structure from transition path sampling simulations are also greater than the ideal distances. Our subsequent quantum/classical mechanism calculations reduced these values only slightly and suggested that these results are not force field artifacts (*28*); instead, from new energetic analysis involving adiabatic minimization (Appendix B of the Supporting Information), we conclude that additional active site rearrangements must follow to evolve the system to a state compatible with the chemical reaction. We term these additional subtle rearrangements in the active site contents the "prechemistry avenue". Such subtle conformational adjustments are consistent with those observed in the structure of a complete substrate complex of pol β when the catalytic Mg^{2+} binds (*73*).

These adiabatic minimizations produce approximate energy landscapes (Figure 6, {*A*,*B*} energy maps for three values of *C*) that allow the system to begin chemistry. Results suggest that (1) the ideal geometry for chemistry (X barrier in the top diagram) has a relatively higher energy with respect to other minima and thus can be considered a true transition

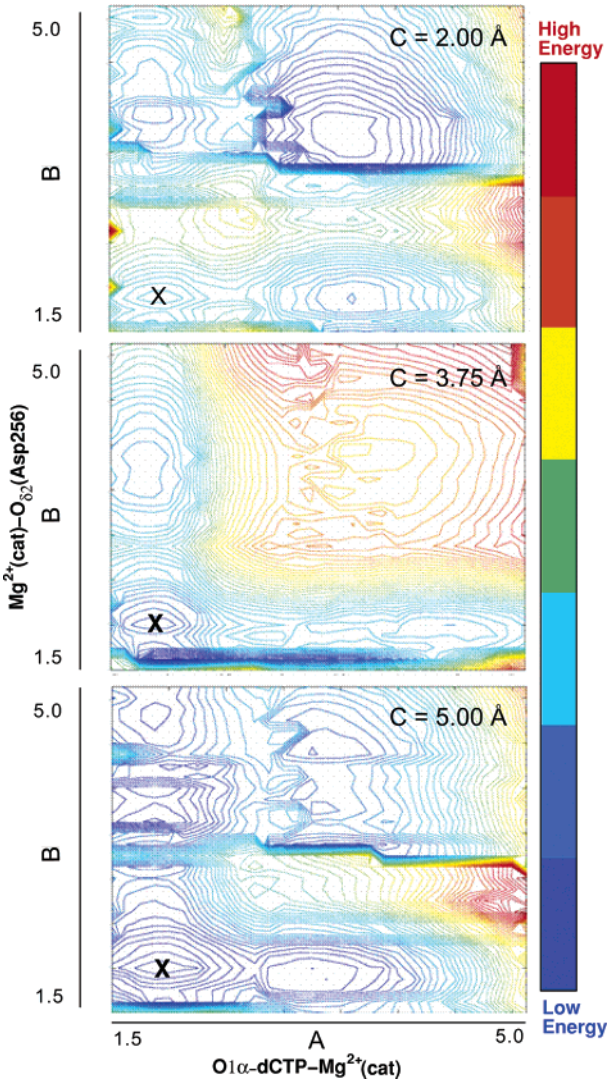

FIGURE 6: Potential energy landscapes (for the G·C system) in the {*A*, *B*} coordinates for three values of *C* as constructed from a series of minimizations in which *A*, *B*, and *C* distances (as defined in the text) were simultaneously constrained. The low-energy regions appear in dark blue; the high-energy regions appear in red. The basin closest to the idealized geometry of the transition state (*14*) is marked with an X.

state, (2) other local energy minima must be surpassed to reach this transition state, and (3) these local energy minima are surmounted by an enzyme hopping mechanism among local basins until the system reaches that transition state which directs it to the chemical reaction. In other words, nucleotide incorporation is an activated process that might have deliberately evolved to produce additional checks and balances for monitoring fidelity.

Does experimental evidence exist to support the proposed prechemistry avenue? In collaboration with Wilson et al., the London group recently probed the local dynamic behavior of [*methyl*-^{13}C]Met-labeled pol β (*29*). These solution studies followed the methyl resonances of six methionine residues in response to substrate binding. Employing a dideoxy-terminated primer to prevent nucleotide insertion, they formed an abortive ternary substrate complex. These NMR studies, and also the early Mildvan work (*74*), suggest localized motions proximal to metal-binding ligands and near β/γ-phosphates prior to chemistry but following dNTP binding. Most significantly, large spectral perturbations of

Table 4: Polymerase Residues Categorized According to Interactions with dNTP, Template Residues, or Key Protein Residues

DNA polymerase	k_{pol}[a] (s^{-1})	dNTP interactions				template residue	protein residue	mutants to be studied	ref
		P_α	P_β	P_γ	base				
pol β	10	x	R183, S180	S180, G189	D276	R283	R258, F272	R258A, F272A, R258A/F272A, S180A, R182A, G189D	*7*
Dpo4	7.6	x	R51	T45, R51	A44	A42	x	T45A, R51A	*75*

[a] Kinetic data were obtained from ref *37* for pol β and ref *20* for Dpo4.

two residues (Met155 and Met191) were noted in the transition from an open binary DNA complex to the abortive ternary complex. Since these residues do not directly contact substrates, the perturbations suggest a localized increase in dynamic behavior, especially for Met155, upon formation of the ternary complex. Because Met155 is adjacent to Asp190 and Asp192 (coordinating metal ligands), these localized motions in the absence of chemistry suggest that subtle rearrangements of catalytically important groups occur. Consistent with this point of view is the observation that the crystallographic *B*-factor for Met155 is increased in the ternary complex relative to that observed in the binary DNA complex. Thus, residues that disrupt and/or facilitate coordination of the β- and γ-phosphate (Arg183, Ser180, and Gly189; see Table 4) are implicated in the NMR experiments (*29*) as players in the conformational change.

Moreover, Mildvan also suggested the existence of what we call the prechemistry avenue: "an error prevention or verification step is needed, which follows the binding of the substrate and precedes the primer elongation step" (*74*). He further proposed that coordination of the enzyme-bound metal by the β-phosphate is the key step in activation of the chemical reaction (*74*, *76*, *77*). That competing pathways spur evolution of the active site geometry slowly in a substrate-dependent context (i.e., depending on correct vs incorrect base present) presents an intriguing mechanism for pol β's regulation of fidelity.

Thus, analyzing the notion of a prechemistry avenue can be reduced to understanding how critical distances in the ternary complex evolve and reach ideal values so that chemistry can proceed. Critical distances involve the $P_\alpha-O3'$ distance (primer terminus), the catalytic $Mg^{2+}-O3'$ distance, and O1A coordination with the magnesium ions. Indeed, a high-resolution pol β ternary crystal structure that includes O3′ of the primer terminus indicates that binding of the catalytic Mg^{2+} induces subtle local conformational adjustments that prepare the active site for efficient chemistry (*73*).

Evidence from these results suggests that the evolutionary pressure can lead the enzyme to control the rate of chemistry by stabilizing the conformations at different values of the reaction coordinate distance (in comparison to the transition state), thereby driving the reaction through alternate paths. Our hypothesis regarding the control of fidelity by altering the critical distance between the nucleophilic O3′ oxyanion and P_α of the incoming dNTP in the active site is consistent with the above notion. All evidence thus points to subtle transformations of the active site via prechemistry events that provide additional checks before orchestration of the chemical reaction.

Chemistry Step. The evolution of pol β through the closing conformational avenue and the prechemistry avenue suggests a context-specific orchestration of the active site for the subsequent phosphoryl transfer step or chemistry. Ab initio simulations on pol β fragments (*78*, *79*) suggested an associative mechanism for the chemical reaction. Rittenhouse et al. (*79*) proposed an initial proton transfer from the 3′-OH group (primer) to $O(P_\alpha)$, and Abashkin et al. (*78*) focused on various protonation possibilities and mentioned that additional protonation states in the active site are possible, especially at the Asp256 site. The availability of high-resolution crystal complexes of pol β has made possible the extension of these studies to a full quantum mechanics/molecular mechanics (QM/MM) treatment which generally includes effects arising from entropic contributions, explicit solvation, long-range electrostatics, and coupling to protein backbone motions. Our 2005 study based on QM/MM minimization (*28*) suggested that two crystallographic water molecules could be involved in the proton transfer to Asp256 from the 3′-OH primer. Clearly, various mechanisms involving proton transfer are possible and may be dependent on the initial protonation states of the conserved aspartate triad in pol β's active site and on the initial model.

Two new QM/MM studies on pol β have just been completed (*80*, *81*) and reported two possible mechanisms differing in the initial proton transfer step.

The former reports favorable mechanisms for the pol β-catalyzed phosphoryl transfer reactions corresponding to both correct (G·C) and incorrect (G·A) nucleotide incorporations in the DNA by using a novel QM/MM protocol involving energy minimizations, dynamics simulations, and quasi-harmonic free energy calculations. The series of transient intermediates in the phosphoryl transfer pathways for both systems suggest a Grotthuss hopping mechanism of proton transfer between water molecules and the three conserved aspartate residues in pol β's active site (see Figure 7) (*80*).

Specifically, for the G·C system, the activation event for the phosphoryl transfer coincides with a reduction in both the $O3'-P_\alpha$ and $O3'-Mg^{2+}$(cat) distances and is accompanied by the transfer of proton of the 3′-OH group to a water dimer; this proton transfer is mediated by the stabilization of a hydrogen bond involving the departed proton and O5′ of dCTP. The bridging water molecule is also hydrogen bonded to a neighboring water molecule, which itself forms two hydrogen bonds to the oxygen atoms of Asp256 (OD2) and Asp192 (OD1), respectively. The $O3'-P_\alpha$ distance and the $P_\alpha-O3A$ distances are both 1.9 Å, and the geometry around P_α is the classic trigonal−bipyramidal configuration with a perfect in-line $O3'-P_\alpha-O3A$ attack angle of 180°. The next two intermediate states correspond to the hopping of the proton from water to OD1 of Asp192 and then to OD2 of Asp192. The latter hop coincides with the cleaving of the $P_\alpha-O3A$ bond, which results in a bond distance of 2.41 Å. (The $O3'-P_\alpha$ distance at this configuration is 1.70 Å.) The sequence of proton hops continues to yield the final

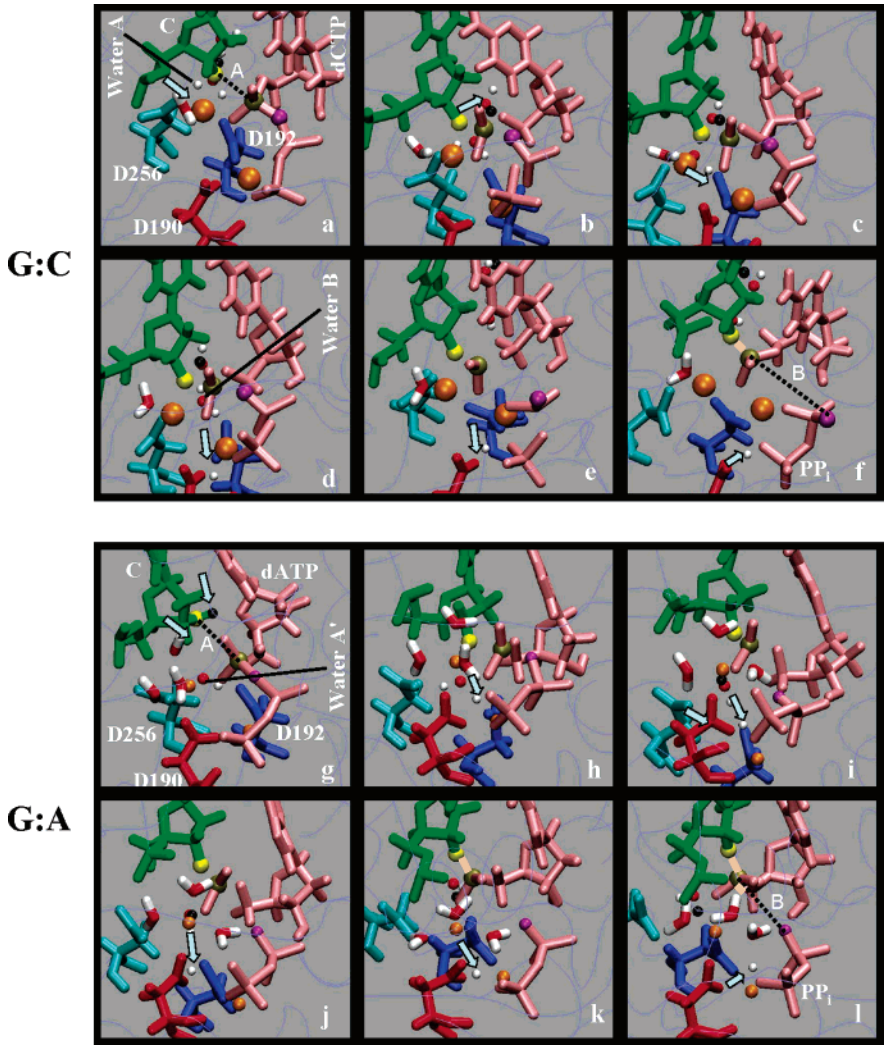

FIGURE 7: Intermediates for pol β's phosphoryl transfer in the G·C (a−f) and G·A (g−l) systems (*80*). Key distances *A* (O3′−P_α) and *B* (P_α−O3A) are provided. (a) G·C system reactant state, for which $A = 2.90$ Å and $B = 1.7$ Å. (b) First intermediate, for which $A = 1.94$ Å and $B = 1.97$ Å. (c) Second intermediate, for which $A = 1.73$ Å and $B = 2.0$ Å. (d) Third intermediate, for which $A = 1.73$ Å and $B = 2.41$ Å. (e) Fourth intermediate, for which $A = 1.70$ Å and $B = 5.53$ Å. (f) G·C product, for which $A = 1.70$ Å and $B = 5.8$ Å. (g) G·A reactant state, for which $A = 6.80$ Å and $B = 1.69$ Å. (h) First intermediate, for which $A = 2.20$ Å and $B = 1.80$ Å. (i) Second intermediate, for which $A = 1.73$ Å and $B = 3.76$ Å. (j) Third intermediate, for which $A = 1.69$ Å and $B = 3.92$ Å. (k) Fourth intermediate, for which $A = 1.68$ Å and $B = 4.03$ Å. (l) G·A product, for which $A = 1.68$ Å and $B = 4.2$ Å. The colors represent D256 (cyan), D190 (red), D192 (blue), dCTP (pink), CYT, terminal DNA primer (green), the O3′H proton (black), O3′ of the attacking nucleophile (yellow), the central phosphorus (tan), leaving O3A (purple), and Mg^{2+} (orange). The O and H atoms of water molecules are colored red and white, respectively. The arrows denote the location and direction of proton hop.

two intermediates, first to OD1 of Asp190 and finally to O1G of PP_i. Along this pathway, the rate-limiting step is the initial reduction of the O3′−P_α distance that triggers the first proton hop, with a free energy of activation of at least 17 kcal/mol, which corresponds closely to measured k_{pol} values. The mechanism of in-line attack is described largely as associative (*80*).

The pathway for the mismatched G·A system reveals a similar sequence of successive proton hops mediating phosphoryl transfer. However, the geometry of the initial (reactant) state is much less ideal with an O3′−P_α distance at 6.87 Å versus a distance of 2.9 Å for the G·C pair, suggesting a higher free energy barrier of at least 21 kcal/mol (*80*).

Another possible mechanism was reported by Lin et al. (*81*) using a constrained minimization QM/MM approach with a different QM/MM interface and a different molecular mechanics force field. The salient features of the pathway in ref *81* include a direct transfer of the proton from O3′ of the terminal DNA primer to the oxygen of Asp256 (occurring at a O3′−P_α distance of 3.5 Å) and an asymmetric in-line attack bond distribution of 2.2 Å for the forming bond and 1.9 Å for the cleaving bond at the transition state. A mechanism for the transfer of the proton to the dissociating PP_i was not proposed (*81*).

The similarities between the pathways described in refs *80* and *81* are that the phosphoryl transfer mechanisms in both studies are associative. The differences are in the exact context (O3′−P_α distance and the destination) of the departing O3′ proton. In ref *80*, the O3′−P_α distance at which the deprotonation occurs is 2.0 Å in contrast to a distance of 3.5 Å in ref *81*. It is interesting to note that the pathway described in ref *80* also included the transfer of this proton to Asp256, mediated by a bridging water molecule, as one of two possibilities, the other being transfer to Asp192. However, while the path of the migrating proton to the

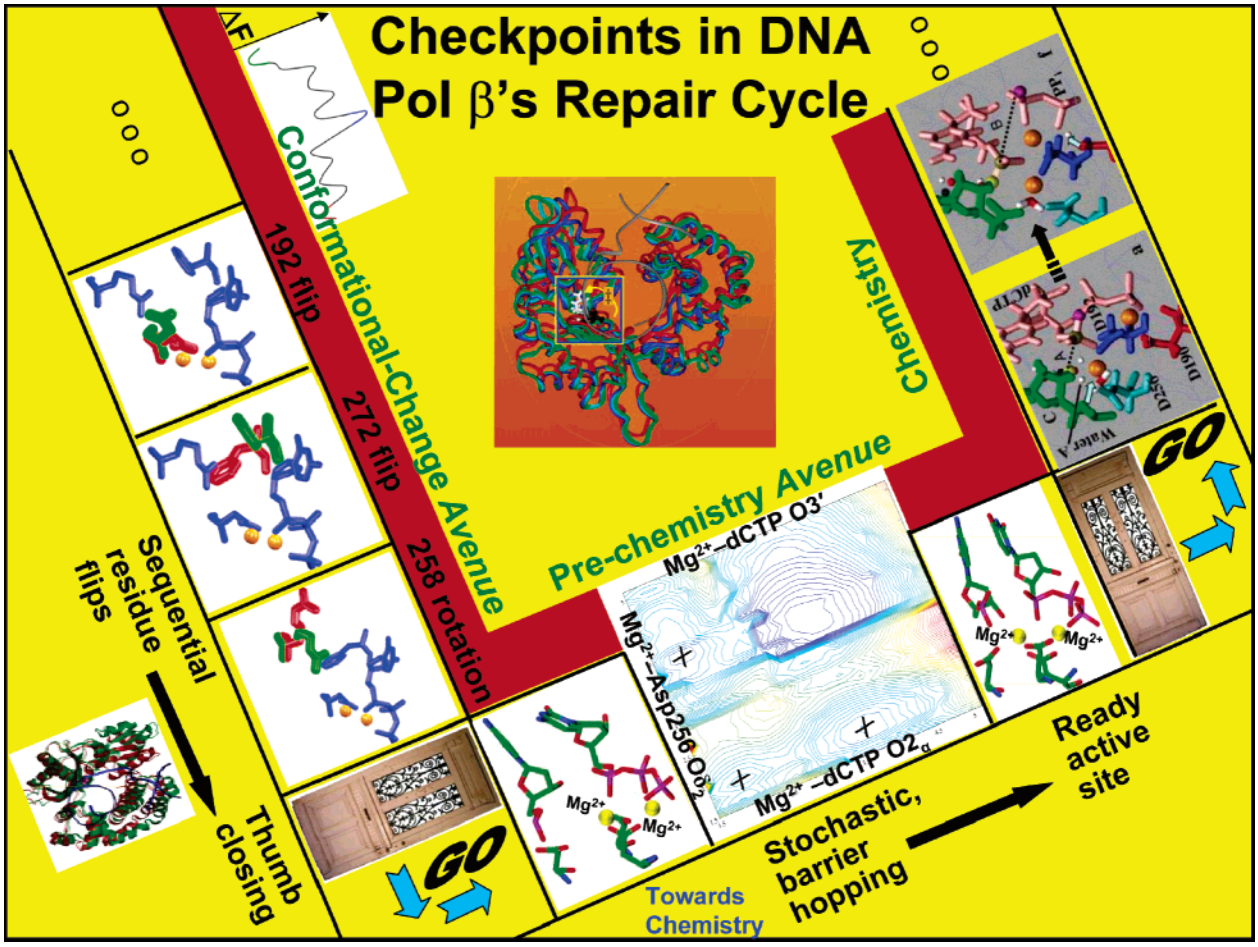

FIGURE 8: Sequential events and corresponding gates controlling pol β's fidelity. Conformational changes upon substrate binding, prechemistry organization of the active site geometry, and chemistry.

Asp192 site was connected (via subsequent Grotthuss hops) to a final proton transfer to PP_i, no such connection was apparent for the proton transferred to Asp256.

CONCLUSIONS

The conformational rearrangements and cooperative motions discussed here likely represent key mechanisms used by polymerases to enhance fidelity. The emerging theme is a relationship between cooperative conformational and chemical activation mechanisms which define gates or kinetic checkpoints in nucleotide incorporation and discrimination processes. Specifically, the works suggest that subdomain motions do not occur as a single concerted event but rather are a sequence of subtle motions that involve key protein residues like Phe272, Arg258, Tyr271, Arg283, Asp192, and Ser180 (see Figures 2 and 4) and the movements of the functional Mg^{2+} ions. These conformational descriptions refine the free energy profiles corresponding to the "conformational change". The corresponding sequence of events (see Figure 2) (*27*, *28*) helps explain how each event contributes to binding and/or catalysis for correct versus incorrect nucleotide insertion. In particular, the comparison between the mismatch (G·A) and matched (G·C) conformational (Figure 2) and chemical (*80*) profiles (Figure 7) reveals systematic differences in the barriers and stability of their closed or initial states that provide insights into fidelity discrimination. Furthermore, the distorted active site geometries in the mismatch systems after the conformational changes, deviating more from the optimal reaction-competent state than the matched cases, imply the likely existence of a postconformational change/prechemistry rearrangement of active site degrees of freedom could serve as a crucial kinetic checkpoint. We term these additional barriers collectively the prechemistry avenue.

Taken together, a landscape of three distinct avenues emerges (Figure 8), each avenue with its own sequence of local changes (involving protein, DNA, ion, and solvent atoms) that affect polymerase efficiency and fidelity: conformational change avenue upon substrate binding, prechemistry avenue to evolve the system to the reaction-competent state, and chemistry avenue for the phosphoryl transfer. This prechemistry avenue is supported by early as well as recent experimental data and may help interpret different polymerase mechanisms through analysis of prechemistry energy barriers. Indeed, data emerging from structural and computational studies of several polymerases (e.g., pol β, pol λ, pol X, and Dpo4) in binary and ternary states emphasize that polymerase conformational changes can vary significantly among polymerases, even within the same family. Thus, polymerases appear to lack a unified description based on the subdomain motions alone to explain their wide variation in DNA synthesis and repair fidelities. However, by invoking the new concept of prechemistry avenue, we may be able to reconcile some observed differences in the fidelities among polymerases.

For example, from simulation studies on pol β (*27*, *33*), pol X (*39*), pol λ (*41*), and Dpo4 (*82*, *83*), it becomes evident that even enzymes that display different degrees of conformational changes upon binding the correct incoming nucleotide do not yet attain the requisite geometry for the chemical reaction following the conformational changes. Moreover, though local distortions vary, the relatively high-fidelity polymerases like pol β have less distorted geometries compared to the low-fidelity polymerase Dpo4 (*33*, *82*, *83*). Thus, in the scenario in which conformational changes involved are fast (not rate-limiting) in the overall insertion pathway, and the intermediate steps on the misincorporation pathway have higher free energies than those on the correct nucleotide incorporation pathway of the same polymerase, differences in energy barriers involved in pushing the polymerase into the perfect geometry (prechemistry step) for the correct and incorrect nucleotide insertion may help interpret variation in fidelities (see the discussion in refs *31* and *84*).

For many polymerases, the rate-limiting step in the misincorporation cycle is the chemical step. Mechanistic details of this phosphoryl transfer reaction are not yet known, especially in a misincorporated active site. Hence, our understanding of the fidelity mechanisms is only partially complete. Since transient states are elusive to traditional structural biology approaches, new techniques that complement the traditional approaches, such as NMR (*29*) and single-molecule studies (*85*, *86*), are required to gain atomic-level insights. Complementary molecular dynamics and energetic studies can help dissect the roles of key molecular components in the polymerase function; specific differences in kinetic profiles for matched versus mismatched base pairs can help relate the induced-fit paradigm to fidelity.

Future simulations and spectroscopic experiments in this direction will undoubtedly confirm some expectations while also revealing surprises. More generally, improving technologies and experimental and simulation studies on the wild-type enzyme and mutants in a variety of template and incoming nucleotide contexts will continue to dissect and combine details of the conformational change, prechemistry, and chemistry avenues and relate these processes to fidelity discrimination mechanisms.

ACKNOWLEDGMENT

We thank Eric Waters and Diana Nguyen who helped with computing energy landscapes for the prechemistry avenue analyses in Figure 6 and Appendix B of the Supporting Information under undergraduate support from the HHMI Summer School at New York University and the NYU Sackler Summer Program in Structural Biology. Computing resources provided by the NCSA supercomputing center are greatly appreciated.

SUPPORTING INFORMATION AVAILABLE

Study of the R258A mutation in DNA polymerase β (Appendix A) and the prechemistry avenue (Appendix B). This material is available free of charge via the Internet at http://pubs.acs.org.

REFERENCES

1. Friedberg, E. C. (2003) DNA damage and repair, *Nature 421* (6921), 436−440.
2. Lindhal, T. (2000) Suppression of spontaneous mutagenesis in human cells by DNA base excision-repair, *Mutat. Res. 462*, 129−135.
3. Seeberg, E., Eide, L., and Bjoras, M. (1995) The base excision repair pathway, *Trends Biochem. Sci. 20*, 391−397.
4. Beard, W. A., et al. (2002) Efficiency of correct nucleotide insertion governs DNA polymerase fidelity, *J. Biol. Chem. 277* (49), 47393−47398.
5. Doublie, S., et al. (1998) Crystal structure of a bacteriophage T7 DNA replication complex at 2.2 angstrom resolution, *Nature 391* (6664), 251−258.
6. Kiefer, J. R., et al. (1998) Visualizing DNA replication in a catalytically active *Bacillus* DNA polymerase crystal, *Nature 391* (6664), 304−307.
7. Sawaya, M. R., et al. (1997) Crystal structures of human DNA polymerase β complexed with gapped and nicked DNA: Evidence for an induced fit mechanism, *Biochemistry 36* (37), 11205−11215.
8. Koshland, D. E. (1995) The key-lock theory and the induced fit theory, *Angew. Chem., Int. Ed., 33* (23−24), 2375−2378.
9. Krahn, J. M., Beard, W. A., and Wilson, S. H. (2004) Structural insights into DNA polymerase β deterrents for misincorporation support an induced-fit mechanism for fidelity, *Structure 12* (10), 1823−1832.
10. Joyce, C. M., and Benkovic, S. J. (2004) DNA polymerase fidelity: Kinetics, structure, and checkpoints, *Biochemistry 43* (45), 14317−14324.
11. Steitz, T. A., et al. (1994) A unified polymerase mechanism for nonhomologous DNA and RNA-polymerases, *Science 266* (5193), 2022−2025.
12. Steitz, T. A. (1999) DNA polymerases: Structural diversity and common mechanisms, *J. Biol. Chem. 274* (25), 17395−17398.
13. Steitz, T. A. (1993) DNA-dependent and RNA-dependent DNA-polymerases, *Curr. Opin. Struct. Biol. 3* (1), 31−38.
14. Lahiri, S. D., et al. (2203) The pentacovalent phosphorus intermediate of a phosphoryl transfer reaction, *Science, 299* (5615), 2067−2071.
15. Stahley, M. R., and Strobel, S. A. (2005) Structural evidence for a two-metal-ion mechanism of group I intron splicing, *Science 309* (5740), 1587−1590.
16. Showalter, A. K., and Tsai, M. D. (2002) A reexamination of the nucleotide incorporation fidelity of DNA polymerases, *Biochemistry 41* (34), 10571−10576.
17. Herschlag, D., Piccirilli, J. A., and Cech, T. R. (1991) Ribozyme-catalyzed and nonenzymatic reactions of phosphate diesters: Rate effects upon substitution of sulfur for a nonbridging phosphoryl oxygen atom, *Biochemistry 30* (20), 4844−4854.
18. Arndt, J. W., et al. (2001) Insight into the catalytic mechanism of DNA polymerase β: Structures of intermediate complexes, *Biochemistry 40* (18), 5368−5375.
19. Dunlap, C. A., and Tsai, M. D. (2002) Use of 2-aminopurine and tryptophan fluorescence as probes in kinetic analyses of DNA polymerase β, *Biochemistry 41* (37), 11226−11235.
20. Fiala, K. A., and Suo, Z. (2004) Mechanism of DNA polymerization catalyzed by *Sulfolobus solfataricus* P2 DNA polymerase IV, *Biochemistry 43* (7), 2116−2125.
21. Hsieh, J. C., Zinnen, S., and Modrich, P. (1993) Kinetic mechanism of the DNA-dependent DNA polymerase activity of human immunodeficiency virus reverse transcriptase, *J. Biol. Chem. 268* (33), 24607−24613.
22. Johnson, K. A. (1993) Conformational coupling in DNA-polymerase fidelity, *Annu. Rev. Biochem. 62*, 685−713.
23. Kunkel, T. A., and Bebenek, R. (200) DNA replication fidelity, *Annu. Rev. Biochem. 69*, 497−529.
24. Patel, P. H., et al. (2001) Prokaryotic DNA polymerase I: Evolution, structure, and "base flipping" mechanism for nucleotide selection, *J. Mol. Biol. 308* (5), 823−837.
25. Li, Y., and Waksman, G. (2001) Structural studies of the Klentaq1 DNA polymerase, *Curr. Org. Chem. 5* (8), 871−883.
26. Yang, L. J., et al. (2002) Polymerase β simulations suggest that Arg258 rotation is a slow step rather than large subdomain motions per se, *J. Mol. Biol. 317* (5), 651−671.
27. Radhakrishnan, R., and Schlick, T. (2004) Orchestration of cooperative events in DNA synthesis and repair mechanism unraveled by transition path sampling of DNA polymerase β's closing, *Proc. Natl. Acad. Sci. U.S.A. 101* (16), 5970−5975.
28. Radhakrishnan, R., and Schlick, T. (2005) Fidelity discrimination in DNA polymerase β: Differing closing profiles for a mismatched

G:A versus matched G:C basepair, *J. Am. Chem. Soc. 127*, 13245−13252.
29. Bose-Basu, B., et al. (2004) Dynamic characterization of a DNA repair enzyme: NMR studies of methyl-C-13 methionine-labeled DNA polymerase β, *Biochemistry 43* (28), 8911−8922.
30. Kirby, T. W., DeRose, E. F., Beard, W. A., Wilson, S. H., and London, R. E. (2005) A thymine isostere in the templating position disrupts assembly of the closed DNA polymerase β ternary complex, *Biochemistry 44*, 15230−15237.
31. Arora, K., et al. (2005) Mismatch-induced conformational distortions in polymerase β/DNA complex support an induced-fit mechanism for fidelity, *Biochemistry 44*, 13328−13341.
32. Arora, K., and Schlick, T. (2005) Conformational transition pathway of polymerase β/DNA upon binding correct incoming substrate, *J. Phys. Chem. B 109* (11), 5358−5367.
33. Arora, K., and Schlick, T. (2004) In silico evidence for DNA polymerase-β's substrate-induced conformational change, *Biophys. J. 87* (5), 3088−3099.
34. Yang, L. J., et al. (2004) Critical role of magnesium ions in DNA polymerase β's closing and active site assembly, *J. Am. Chem. Soc. 126* (27), 8441−8453.
35. Yang, L. J., et al. (2004) Highly organized but pliant active site of DNA polymerase β: Compensatory mechanisms in mutant enzymes revealed by dynamics simulations and energy analyses, *Biophys. J. 86* (6), 3392−3408.
36. Yang, L. J., et al. (2002) Local deformations revealed by dynamics simulations of DNA polymerase β with DNA mismatches at the primer terminus, *J. Mol. Biol. 321* (3), 459−478.
37. Vande Berg, B. J., Beard, W. A., and Wilson, S. H. (2001) DNA structure and aspartate 276 influence nucleotide binding to human DNA polymerase β: Implication for the identity of the rate-limiting conformational change, *J. Biol. Chem. 276* (5), 3408−3416.
38. Beard, W. A., Shock, D. D., and Wilson, S. H. (2004) Influence of DNA structure on DNA polymerase β active site function: Extension of mutagenic DNA intermediates, *J. Biol. Chem. 279* (30), 31921−31929.
39. Sampoli Benitez, B., Arora, K., and Schlick, T. (2006) In silico studies of the African swine fever virus DNA polymerase X support an induced-fit mechanism, *Biophys. J. 90* (1), 42−56.
40. Maciejewski, M. W., et al. (2001) Solution structure of a viral DNA repair polymerase, *Nat. Struct. Biol. 8* (11), 936−941.
41. Foley, M. C., Arora, K., and Schlick, T. (2006) Sequential side-chain residue transitions produce the ternary state from the binary state of DNA polymerase λ, *Biophys. J. 91*, 3182−3195.
42. Johnson, S. J., and Beese, L. S. (2004) Structures of mismatch replication errors observed in a DNA polymerase, *Cell 116* (6), 803−816.
43. Batra, V. K., et al. (2005) Nucleotide-induced DNA polymerase active site motions accomodating a mutagenic DNA intermediate, *Structure 13*, 1225−1233.
44. Shah, A. M., et al. (2001) Y265H mutator mutant of DNA polymerase β: Proper geometric alignment is critical for fidelity, *J. Biol. Chem. 276* (14), 10824−10831.
45. Florian, J., Goodman, M. F., and Warshel, A. (2003) Computer simulation of the chemical catalysis of DNA polymerases: Discriminating between alternative nucleotide insertion mechanisms for T7 DNA polymerase, *J. Am. Chem. Soc. 125* (27), 8163−8177.
46. Kool, E. T. (2002) Active site tightness and substrate fit in DNA replication, *Annu. Rev. Biochem. 71* (1), 191−219.
47. Moran, S., Ren, X. F., and Kool, E. T. (1997) A thymidine triphosphate shape analog lacking Watson-Crick pairing ability is replicated with high sequence selectivity, *Proc. Natl. Acad. Sci. U.S.A. 94*, 10506−10511.
48. Morales, J. C., and Kool, E. T. (2000) Varied Molecular Interactions at the Active Sites of Several DNA Polymerases: Nonpolar Nucleoside Isosteres as Probes, *J. Am. Chem. Soc. 122*, 1001−1007.
49. Xiang, Y., Oelschlaeger, P.; Florian, J., Goodman, M. F., and Warshel, A. (2006) Simulating the effect of DNA polymerase mutations on transition-state energetics and fidelity: Evaluating amino acid group contribution and allosteric coupling for ionized residues in human pol β, *Biochemistry 45* (23), 7036−7048.
50. Beard, W. A., and Wilson, S. H. (2006) Structure and mechanism of DNA polymerase β, *Chem. Rev. 106*, 361−382.
51. Kim, S. J., et al. (2003) Rapid segmental and subdomain motions of DNA polymerase β, *J. Biol. Chem. 278* (7), 5072−5081.
52. Rothwell, P. J., Mitaksov, V., and Waksman, G. (2005) Motions of the fingers subdomain of Klentaq1 are fast and not rate limiting: Implications for the molecular basis of fidelity in DNA polymerases, *Mol. Cell 19* (3), 345−355.
53. Garcia-Diaz, M., et al. (2005) A closed conformation for the Pol λ catalytic cycle, *Nat. Struct. Mol. Biol. 12* (1), 97−98.
54. Kraynov, V. S., et al. (1997) DNA polymerase β: Analysis of the contributions of tyrosine-271 and asparagine-279 to substrate specificity and fidelity of DNA replication by pre-steady-state kinetics, *Biochem. J. 323*, 103−111.
55. Date, T., et al. (1990) Site-directed mutagenesis of recombinant rat DNA polymerase β: Involvement of arginine-183 in primer recognition, *Biochemistry 29*, 5027−5034.
56. Date, T., et al. (1991) Aspartic acid residues at positions 190 and 192 of rat DNA polymerase β are involved in primer binding, *Biochemistry 30*, 5286−5292.
57. Menge, K. L., et al. (1995) Structure-function analysis of the mammalian DNA polymerase β active site: Role of aspartic acid 256, arginine 254, and arginine 258 in nucleotidyl transfer, *Biochemistry 34* (49), 15934−15942.
58. Opresko, P. L., Sweasy, J. B., and Eckert, K. A. (1998) The mutator form of polymerase β with amino acid substitution at tyrosine 265 in the hinge region displays an increase in both base substitution and frame shift errors, *Biochemistry 37*, 2111−2119.
59. Shah, A. M., Maitra, M., and Sweasy, J. B. (2003) Variants of DNA polymerase β extend mispaired DNA due to increased affinity for nucleotide substrate, *Biochemistry 42* (36), 10709−10717.
60. Beard, W. A., and Wilson, S. H. (1998) Structural insights into DNA polymerase β fidelity: Hold tight if you want it right, *Chem. Biol. 5* (1), R7−R13.
61. Beard, W. A., et al. (1996) Enzyme-DNA interactions required for efficient nucleotide incorporation and discrimination in human DNA polymerase b, *J. Biol. Chem. 271* (21), 12141−12144.
62. Li, S. X., Vaccaro, J. A., and Sweasy, J. B. (1999) Involvement of phenylalanine 272 of DNA polymerase β in discriminating between correct and incorrect deoxynucleoside triphosphates, *Biochemistry 38*, 4800−4808.
63. Skandalis, A., and Loeb, L. A. (2001) Enzymatic properties of rat DNA polymerase β mutants obtained by randomized mutagenesis, *Nucleic Acids Res. 29*, 2418−2426.
64. Ahn, J., Werneburg, B. G., and Tsai, M. D. (1997) DNA polymerase b: Structure-fidelity relationship from pre-steady-state kinetic analyses of all possible correct and incorrect base pairs for wild type and R283A mutant, *Biochemistry 36* (5), 1100−1107.
65. Werneburg, B. G., et al. (1996) DNA polymerase β: Pre-steady-state kinetic analysis and roles of arginine-283 in catalysis and fidelity, *Biochemistry 35* (22), 7041−7050.
66. Humphrey, W., Dalke, A., and Schulten, K. (1996) VMD: Visual molecular dynamics, *J. Mol. Graphics 14* (1), 33−38.
67. Sirover, M. A., and Loeb, L. A. (1976) Infidelity of DNA-synthesis in vitro: Screening for potential metal mutagens or carcinogens, *Science 194*, 1434−1436.
68. Wang, J., et al. (1997) Crystal structure of a pol a family replication DNA polymerase from bacteriophage RB69, *Cell 89* (7), 1087−1099.
69. Garcia-Viloca, M., and Gao, J. L. (2004) Generalized hybrid orbital for the treatment of boundary atoms in combined quantum mechanical and molecular mechanical calculations using the semiempirical parameterized model 3 method, *Theor. Chem. Acc. 111* (2−6), 280−286.
70. Washel, A. (1989) *Computer modeling of chemical reactions in enzymes and solution*, John Wiley and Sons, New York.
71. Bakhtina, M., et al. (2005) Use of viscogens, dNTPaS, and rhodium(III) as probes in stopped flow experiments to obtain new evidence for the mechanism of catalysis by DNA polymerase β, *FASEB J. 19* (5), A1402−A1402.
72. Webster, C. E. (2004) High-energy intermediate or stable transition state analogue: Theoretical perspective of the active site and mechanism of β-phosphoglucomutase, *J. Am. Chem. Soc. 126* (22), 6840−6841.
73. Batra, V. K., et al. (2006) Magnesium-induced assembly of a complete DNA polymerase catalytic complex, *Structure 14* (4), 757−766.
74. Ferrin, L. J., and Mildvan, A. S. (1986) NMR-studies of the conformations and interactions of substrates and ribonucleotide templates bound to the large fragment of DNA-polymerase-I, *J. Cell. Biochem.*, 125.

75. Ling, H., et al. (2001) Crystal structure of a Y-family DNA polymerase in action: A mechanism for error-prone and lesion-bypass replication, *Cell 107* (1), 91−102.
76. Mildvan, A. S. (1997) Mechanisms of signaling and related enzymes, *Proteins 29* (4), 401−416.
77. Bolton, E. C., Mildvan, A. S., and Boeke, J. D. (2002) Inhibition of reverse transcription in vivo by elevated manganese ion concentration, *Mol. Cell 9* (4), 879−889.
78. Abashkin, Y. G., Erickson, J. W., and Burt, S. K. (2001) Quantum chemical investigation of enzymatic activity in DNA polymerase β. A mechanistic study, *J. Phys. Chem. B 105*, 287−292.
79. Rittenhouse, R. C., et al. (2003) Characterization of the active site of DNA polymerase β by molecular dynamics and quantum chemical calculation, *Proteins: Struct., Funct., Genet. 53*, 667−682.
80. Radhakrishnan, R., and Schlick, T. (2006) Correct and incorrect nucleotide incorporation pathways in DNA polymerase β, *Biochem. Biophys. Res. Commun. 250*, 521−529.
81. Lin, P., et al. (2006) Energy analysis of chemistry for correct insertion by DNA polymerase β, *Proc. Natl. Acad. Sci. U.S.A. 103*, 13294−13299.
82. Wang, L. H., and Broyde, S. (2006) A new anti conformation for N-(deoxyguanosin-8-yl)-2-acetylaminofluorene (AAF-dG) allows Watson-Crick pairing in the *Sulfolobus solfataricus* P2 DNA polymerase IV (Dpo4), *Nucleic Acids Res. 34* (3), 785−795.
83. Wang, L. H., et al. (2005) Accommodation of a 1S-(−)-Benzo-[c]phenanthrenyl-N-6-dA adduct in the Y-family Dpo4 DNA polymerase active site: Structural insights through molecular dynamics simulations, *Chem. Res. Toxicol. 18* (3), 441−456.
84. Arora, K. (2006) A computational investigation of the conformational transitions in DNA polymerases (pol β, pol X, pol λ, and Dpo4): Implication for DNA synthesis and repair fidelity, Ph.D. Thesis, p 299, New York University, New York.
85. Bustamante, C., Bryant, Z., and Smith, S. B. (2003) Ten years of tension: Single-molecule DNA mechanics, *Nature 421* (6921), 423−427.
86. Wuite, G. J. L., et al. (2000) Single-molecule studies of the effect of template tension on T7 DNA polymerase activity, *Nature 404* (6773), 103−106.

BI061353Z